

RadYOLOLet: Radar Detection and Parameter Estimation Using YOLO and WaveLet

Shamik Sarkar, *Member, IEEE*, Dongning Guo, *Fellow, IEEE*, and Danijela Cabric, *Fellow, IEEE*

Abstract—Detection of radar signals without assistance from the radar transmitter is a crucial requirement for emerging and future shared-spectrum wireless networks like Citizens Broadband Radio Service (CBRS). In this paper, we propose a supervised deep learning-based spectrum sensing approach called RadYOLOLet that can detect low-power radar signals in the presence of interference and estimate the radar signal parameters. The core of RadYOLOLet is two different convolutional neural networks (CNN), RadYOLO and Wavelet-CNN, that are trained independently. RadYOLO operates on spectrograms and provides most of the capabilities of RadYOLOLet. However, it suffers from low radar detection accuracy in the low signal-to-noise ratio (SNR) regime. We develop Wavelet-CNN specifically to deal with this limitation of RadYOLO. Wavelet-CNN operates on continuous Wavelet transform of the captured signals, and we use it only when RadYOLO fails to detect any radar signal. We thoroughly evaluate RadYOLOLet using different experiments corresponding to different types of interference signals. Based on our evaluations, we find that RadYOLOLet can achieve 100% radar detection accuracy for our considered radar types up to 16 dB SNR, which cannot be guaranteed by other comparable methods. RadYOLOLet can also function accurately under interference up to 16 dB SINR.

Index Terms—Spectrum Sensing, Radar Detection, Deep Learning, YOLO, Wavelet Transform, Spectrum Sharing.

I. INTRODUCTION

Motivation: Radar bands are increasingly being shared by mobile broadband systems for better radio spectrum utilization via dynamic spectrum access [1]. One such well-known spectrum-sharing paradigm in the United States is CBRS [2]. Hence, robust spectrum sensing methods for detecting radar signals are of prime importance. In such spectrum sensing problems, the sensor does not have a priori knowledge of the radar transmitters' signal parameters, transmission activities, and location. Under these restrictions, prior works have shown that machine learning (ML) based spectrum sensing methods can detect radar with high accuracy when the peak radar signal to average interference and noise ratio (SINR)¹ per MHz at the sensor is above 20 dB [3].

This work was supported by SpectrumX, which is an NSF Spectrum Innovation Center funded via Award 2132700.

Shamik Sarkar is with the Electronics and Communications Engineering Department, Indraprastha Institute of Information Technology Delhi, 110020, India. This work was done when Shamik was with UCLA (e-mail: shamik@iitd.ac.in).

Danijela Cabric is with the Electrical and Computer Engineering Department, University of California at Los Angeles, Los Angeles, CA 90095 USA (e-mail: danijela@ee.ucla.edu).

Dongning Guo is with the Electrical and Computer Engineering Department, Northwestern University, Evanston, IL 60208 USA (e-mail: dGuo@northwestern.edu).

¹For brevity, throughout the paper, we will use 'SINR (and SNR)' to imply peak-to-average SINR (and SNR) per MHz.

Goals: Our goal is to push the minimum required radar SINR limit to below 20 dB, at which the radar signals can be detected by the spectrum-sensing sensor (henceforth sensor) with high accuracy. Specifically, we investigate three fundamental aspects of spectrum sensing for radar signals. First, we aim to develop a method to detect low SNR radar signals. Second, we aim to have the capability of detecting radar signals in the presence of interference. Third, while aiming for the above goals, we also want to estimate the parameters of radar and interference signals, e.g., bandwidth, pulse width, pulse interval, etc. These capabilities will be instrumental in designing intelligent and efficient radar-communication spectrum-sharing systems in the future.

For our investigation, we rely on the CBRS framework. CBRS is a complex spectrum-sharing ecosystem with many details [4]. Hence, we enumerate the main features of CBRS that are relevant to our problem. i) We consider five types of radar signals relevant to CBRS. ii) The sensor, known as environmental sensing capability (ESC) in CBRS, must detect the radar signals without assistance from the radar transmitter. iii) The interference at the sensor originates from a cellular network that shares the spectrum with the radar signals. The interference source has no coordination with the radar transmitter. More details about these features are discussed later in Section II. In the current CBRS rules, the sensor must detect the radar signals with high accuracy when the SINR is above 20 dB. However, as mentioned before, we want to go below the 20 dB radar SINR requirement in CBRS without compromising the radar detection accuracy.

Challenges: To achieve our ambitious goals, we must address several important challenges.

- First, our considered radar signals have a low duty cycle, which is the ratio of ON time to OFF time. Thus, it is difficult to detect radar signals using their ON times, which are much smaller than their OFF times. This challenge becomes more critical for low SNR radar.
- Second, the sensor must detect different types of radar signals that are dissimilar from one another and have unknown signal parameters within a range. Hence, it is challenging to have a method that can achieve high detection accuracy on all relevant types of radar signals.
- Third, due to the dissimilarity of the different radar types, their parameters belong to very wide ranges. For example, some radar signals have narrow bandwidth, while some have narrow pulses. Hence, it is difficult to estimate the radar signal parameters accurately.
- Fourth, the interference signals from communication systems do not have a low duty cycle. Consequently, their

presence can significantly degrade the sensor’s ability to detect ephemeral radar signals, especially when the interference-to-noise ratio (INR) is high.

- Fifth, if the interference signals have certain transmission activity patterns, then the sensor must be capable of distinguishing such patterns from those of the radar signals. Otherwise, there will be spurious false alarms, which can hinder the overall goal of spectrum sharing.

Approach: To address the above-mentioned challenges, we propose a supervised deep-learning-based spectrum sensing method called RadYOLOLet. To deal with the first challenge, RadYOLOLet uses two different CNNs. While we develop the first CNN, which we call RadYOLO, to have different necessary capabilities, the second one is built specifically to deal with low SNR radar signals. RadYOLO operates on spectrograms and simultaneously detects the radar signals and estimates their parameters using the YOLO framework [5]. We carefully design the formation of the spectrograms to assist RadYOLO in fulfilling its objectives. By virtue of being a data-driven supervised deep learning method, RadYOLO has the capability of detecting different types of radar signals using the same neural network and, thus, overcomes the second challenge. In RadYOLO, we take the ambitious step of treating each radar pulse as a different object, detecting, and localizing them. This enables us to deal with the third challenge. This approach also helps us counter the fourth challenge as it provides robustness against interference signals that switch between the ON and OFF phases. We develop several strategies to tackle the small-sized radar pulse objects in RadYOLO. RadYOLO treats radar and interference signals as different classes and learns to distinguish between their patterns, which is crucial for tackling the fifth challenge. Finally, RadYOLO can also extract the parameters of the interference signals.

However, RadYOLO is not robust in detecting radar in the low SNR regime. Hence, we use the second CNN, which operates on images generated by Wavelet transform of the captured signals. We call this CNN Wavelet-CNN. Here our intuition is to leverage Wavelet transform, which has been used as a robust method for detecting low SNR radar echoes in traditional radar signal processing [6], where the receiver is aware of the radar signal parameters. However, in our case, the radar signal detection problem is more complex as the sensor is unaware of the transmitted radar signals. Hence, we use a neural network for the detection task. Instead of directly using a Wavelet transformed signal as input to the CNN, we carefully design a preprocessing step before the Wavelet transforms that improves our chances of detecting radar signals. Wavelet-CNN acts as a binary classifier that distinguishes between radar and non-radar signals. Thus, Wavelet-CNN lacks the diversity (multi-class classification and signal parameter estimation) of RadYOLO. For this reason, we use Wavelet-CNN only when RadYOLO does not detect any radar. While Wavelet-CNN provides robustness to low SNR radar, it does not provide robustness to interference inherently. Hence, we develop several strategies in Wavelet-CNN and its associated preprocessing such that it does not miss-classify interference signals as radar.

A. Related Work

In traditional monostatic radar, the radar transmitter emits pulses that are reflected by objects, received by the radar receiver, and processed for detecting the objects. An essential signal processing tool in this scheme is matched filtering of the received signal for improving the SNR of the reflected pulses [8]. However, matched filtering-based techniques are not applicable in scenarios where the spectrum sensing sensor is unaware of the transmitted signal parameters.

To deal with interference, MIMO radars use beamforming methods like sampled matrix inversion (SMI) based minimum variance distortionless response (MVDR) [9] or ML-based MVDR for suppressing interference [10]. However, we cannot directly apply such beamforming techniques to our problem as the radar and interference signals arrive at the sensor antenna from opposite directions [11]². Additionally, having an antenna array on the sensor can impact the location privacy (via the direction of arrival estimate) of navy radar transceivers [4].

Electronic support and electronic intelligence (ES/ELINT) is a broad area where the task is to detect radar signals that have a low probability of intercept (LPI) [12]. In such problems, the radar signals are designed to be challenging to detect. The radar detection problem in CBRS differs from ES/ELINT as the radar transmitter is not trying to hide its signals from the sensor. However, LPI radar detection techniques can be leveraged in our problem.

Since the inception of the idea of ESC in CBRS, there have been several works on detecting radar signals [3], [7], [13]–[16]. Most of these works have relied on ML-based spectrum sensing. These methods generally frame the radar detection problem as a classification task. Several feature representations and learning methods have been proposed for this problem in the literature. For example, a combination of signal amplitude and phase difference can be used as input to a CNN for predicting the presence of radar signals [13]. Instead of signal amplitude and phase, the classification task can be performed using spectrograms [15]. Computer vision-inspired objection detection methods can be applied to spectrograms for detecting radar signals and estimating their bandwidth [3] or detecting non-radar signals that might be present on the spectrograms [7]. Instead of deep learning, support vector machines (SVM) based classifiers can also be used for the classification task using features like higher-order and peak statistics [16]. As mentioned before, matched filtering is not directly applicable to our problem. However, if only one type of radar signal is considered and the radar pulse shape is assumed to be known at the sensor, then matched filtering can be applied [14]. Unlike RadYOLOLet, none of these works aim at detecting low-power radar signals, estimating their parameters, and tolerating higher interference.

An important component of RadYOLOLet is YOLO-based radar detection. Similar ideas have been explored in a couple of prior works [3], [7]. Hence, we point out the differences between RadYOLOLet and other YOLO-based radar detection

²The source of interference at the sensors in CBRS is unique due to the deployment factors, and it is different from the traditional interference models in radar signal processing. More details can be found in [11].

TABLE I: Comparison of YOLO-based radar detection methods.

Methods	Capabilities								
	Radar detection	All CBRS radar types	Interference detection	Radar bandwidth estimation	Radar pulse parameters estimation	Interference parameters estimation	Tolerance to low radar power	Tolerance to high power interference	Tolerance to different type of interference
RadYOLOLet	YES	YES	YES	YES	YES	YES	YES	YES	YES
DeepRadar [3]	YES	YES	NO	YES	NO	NO	NO	NO	NO
Waldo [7]	YES	NO	YES	YES	NO	NO	NO	YES	NO

works in Table I. We see that our proposed approach has several capabilities that are absent in other YOLO-based radar detection works.

Another vital component of our work is using Wavelet transform for radar detection. Hence, we briefly review the relevant works in this domain. Continuous Wavelet transform (CWT) can be used for low SNR radar target detection and can have better processing gain (input to output SNR ratio) than matched filtering [6]. While this work serves as an important motivation, it cannot be directly applied to our problem as it assumes the knowledge of the transmitted radar signal, does not consider different radar types and interference. Wavelet transform also has the capability of reducing noise, and that can be used as used to denoise the radar returns [17]. Multi-scale product of discrete Wavelet transform can be applied to the power spectral densities (PSD) of the captured signals for noise reduction [18]. However, these approaches differ from ours as we use Wavelet transform to mimic the operation of matched filtering without the cognizance of radar signal parameters. Our idea of using a CNN on images generated via Wavelet transform has similarities with the work in [19]. However, our approach and objectives differ from those in [19]. Specifically, the work in [19] aims at modulation recognition and does not consider the presence of interference. In contrast, our focus is on signal detection rather than modulation classification. Additionally, an important focus of our approach is to deal with interference.

B. Contributions

Our main contributions to this paper are the following.

- 1) We develop a deep learning-based object detection method, RadYOLO, that simultaneously detects radar and interference signals and estimates their parameters. For radar, RadYOLO estimates the center frequency, bandwidth, number of pulses, pulse width, and pulse interval. For interference, RadYOLO estimates center frequency, bandwidth, and ON times.
- 2) We develop a deep learning-based binary classifier, Wavelet-CNN, that distinguishes between radar and non-radar signals, especially in the low radar SNR regime. Wavelet-CNN uses a CNN as its core, operating on the Wavelet transform of the captured signals.
- 3) Our overall design, RadYOLOLet, is a tight integration of RadYOLO and Wavelet-CNN. Wavelet-CNN strives to succeed when RadYOLO fails. At the same time, Wavelet-CNN relies on RadYOLO for signal parameter estimation as Wavelet-CNN cannot do that. Importantly, for both the CNNs, we design several preprocessing and postprocessing of the inputs and outputs, respectively, for achieving robustness to noise and interference.
- 4) We thoroughly evaluate RadYOLOLet using a diverse set of experiments involving different radar SNR and

interference INR scenarios. Our evaluations show that, when interference signals are not present, RadYOLOLet can achieve 100% radar detection accuracy for all five radar types up to 16 dB SNR. In the presence of different types of interference signals, RadYOLOLet can detect radar signals with 100% accuracy up to 16 dB SINR.

C. Organization

In Section II, we present our system model, the detail about the radar signals relevant to our problem, and the problem statement. Then, in Section III, we describe our methodology in RadYOLOLet. In Section IV, we explain our evaluation setup and present our results. Finally, Section V provides conclusions and future work.

II. SYSTEM MODEL

Radar characteristics: As in CBRS, we consider five radar types whose characteristics are shown in Table II. Radar types 1 and 2 are pulse-modulated, and the remaining ones are frequency-chirping. Thus, the bandwidth of radar types 3-5 in Table II are their chirp width.

Sensor details: We consider a sensor whose task is to detect the above-described radar signals with high accuracy and estimate their parameters. For all radar types, the parameters are in a range that is known to the sensor. The radar pulse parameters do not change within a burst (a set of pulses). However, at a particular time, the exact values of these parameters, along with the radar type, are unknown to the sensor. The sensor's task is to detect, at most, one radar signal at a time. I.e., we assume multiple radar signals do not appear simultaneously. Due to the reasons described in Section I-A, we consider the sensor equipped with a single antenna. The instantaneous bandwidth of the sensor is B MHz, and the sampling rate is also B MS/sec. As the radar signals can appear anywhere on a 100 MHz portion of the CBRS band (3550-3650 MHz), ideally, we should have $B \geq 100$. Such sensors have been considered in [3], [7]. An alternative approach is to use $B = 10$, which is what we consider in the work. In this approach, the 100 MHz band can be broken into 10 different non-overlapping 10 MHz sub-bands, and the spectrum sensing algorithm can be applied to each sub-band individually. Then, the decisions for all sub-band can be combined into a single decision for the whole 100 MHz band. Accordingly, without loss of generality, we focus on monitoring a $B = 10$ MHz band for our sensor. Dividing the 100 MHz

TABLE II: Radar signal parameters [20]

Radar type	Pulse width (μ sec)	Inter-pulse interval (msec)	Number of pulses per burst	Burst duration (msec)	Band width (MHz)
1	0.5 - 2.5	0.9 - 1.1	15 - 40	13 - 44	1
2	13 - 52	0.3 - 3.3	5 - 20	1 - 66	1
3	3 - 5	0.3 - 3.3	8 - 24	2 - 80	50 - 100
4	10 - 30	0.3 - 3.3	2 - 8	0.6 - 26	1 - 10
5	50 - 100	0.3 - 3.3	8 - 24	2 - 80	50 - 100

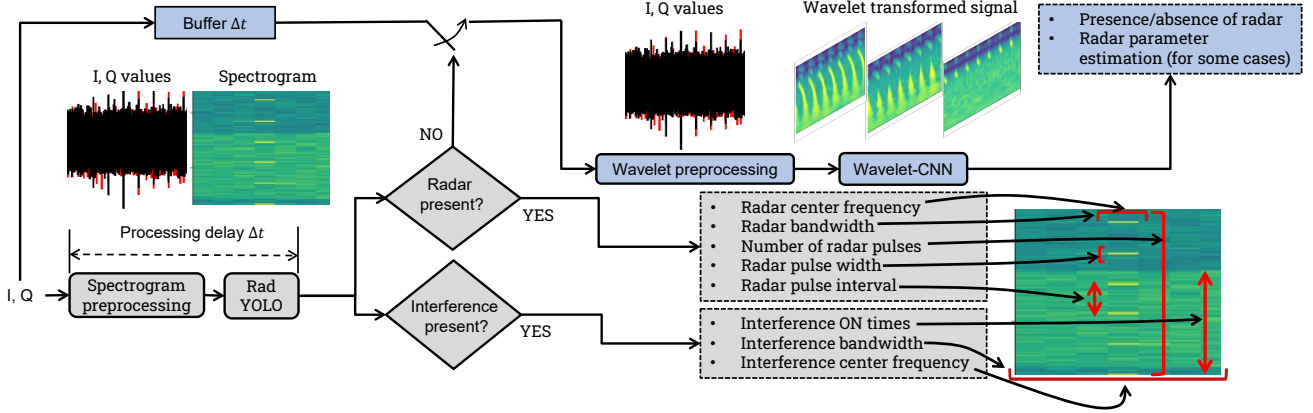


Fig. 1: Overall flow diagram of RadYOLOLet. The switch is closed when the branch labeled ‘NO’ is triggered. For each block, we show on top the form of the signal on which the blocks operate.

band into smaller sub-bands and making independent decisions is computationally more expensive than looking at the whole 100 MHz band altogether and making a single decision. We choose to use the computationally expensive approach as $B = 10$ suites RadYOLOLet better in achieving high radar detection accuracy, as explained later in Section III-C. There is another implication of using $B = 10$. For radar types 3 and 5 (refer to Table II), the signal bandwidth can be larger than 10 MHz. Hence, for these two radar types, we consider only the portion of the radar band that overlaps the sensor’s monitoring bandwidth as the radar bandwidth.

Interference model: The sensor should be able to operate in the presence of interference. However, the interference signals are not adversarial. As in CBRS, the source of interference is a cellular network that shares the spectrum with the radar signals. In our system model, we consider that the source of interference is a cellular base station (BS) whose downlink signals appear at the sensor as interference. Following the most popular channel occupancy of 10 MHz by the cellular operators in CBRS [21], we assume the interference signal occupies the whole 10 MHz band on which the sensor operates. As part of our research in this work, we examine different types of interference signals and their impact on detecting radar signals. Considering the LTE sub-frame duration of 1 msec [22], for all the interference signals considered in this paper, we assume that their ON time is at least 1 msec.

Decision granularity: The sensor must continuously monitor the B MHz band to detect radar signals. The sensor uses the sampled I, Q values from the RF frontend as its observations and makes decisions based on them. We discretize the decisions in contiguous, non-overlapping time windows of duration T msec. I.e., for every batch of $N = (T \times 10^{-3} \times B \times 10^6)$ samples, the sensor makes a decision. The decisions of multiple time windows can be combined to make a single decision over a time duration longer than T msec. However, without loss of generality, we focus on the sensor’s performance on T msec time windows and do not consider combining decisions of multiple time windows. Finally, the sensor has enough computing capabilities to make decisions at a rate that is faster than the sampling rate.

Problem Statement: Our problem is to develop a method that has the following attributes:

- Capability to make accurate radar (possibly low SNR) detection decisions for each time window of duration T msec, both in the presence and absence of interference.
- When a radar signal is detected, the capability to estimate radar center frequency, bandwidth, pulse width, pulse interval, and the number of pulses (within a time window of T msec).
- Capability of detecting interference signals, both in the presence and absence of radar.
- When interference is detected, the capability to estimate its center frequency, bandwidth, and ON times.

While the radar center frequency and bandwidth estimation is an essential in CBRS, the remaining capabilities can serve as general tools of importance in spectrum sensing.

III. DESCRIPTION OF RADYOLOLET

In this section, first, we present the overall flow diagram of RadYOLOLet and then explain its components.

Overview of RadYOLOLet: Fig. 1 shows the flow diagram of RadYOLOLet. The input to RadYOLOLet is a set of I, Q values corresponding to a time window of T msec. We denote the I, Q values as a complex vector s of size N . There are two interdependent flows in Fig. 1.

In the first flow, the I, Q values go through the spectrogram preprocessing block, which generates a spectrogram using the Short-Term Fourier transform (STFT) of the I, Q values. The details of generating the spectrogram are described in Section III-A. The generated spectrogram is used as the input to the RadYOLO block. The RadYOLO block is essentially a CNN inspired by the YOLO framework. RadYOLO takes the spectrogram as input and produces as output its detection decisions, i.e., whether radar and/or interference signals are present or not. If it detects a signal, it also estimates the signal parameters as shown in Fig. 1. The details of the RadYOLO are presented in Section III-B. When RadYOLO detects a radar signal, the second flow comprising of Wavelet preprocessing and Wavelet-CNN blocks in Fig. 1 are not used.

If RadYOLO predicts the absence of radar, the switch in Fig. 1 is closed, and the input I, Q values go through the second flow. When the second flow is used, its output overrides the output of the first flow. The buffer block in Fig. 1 shows

that both the flows operate on the same set of I, Q values, but the second flow is triggered only after the first flow makes its decision. In our second flow, the Wavelet preprocessing block performs frequency domain filtering on the input signal and performs continuous Wavelet transform on each filtered signal. The output of this block gives us three different images, which we stack along the depth dimension and form a 3-D tensor that is fed to the Wavelet-CNN block. The details of the Wavelet preprocessing block are presented in Section III-C. The Wavelet-CNN block, which is a CNN, takes the 3-D tensor as input, acts as a binary classifier, and produces its detection decision regarding the presence of radar signals as output. The details of the Wavelet-CNN block are presented in Section III-D.

A. Spectrogram Preprocessing

The processing in this block is shown in Fig. 2.

Selection of T : First, we form the complex vector \mathbf{s} of size N , which, as defined earlier, is the set of I, Q values corresponding to a time window of T msec. However, we must decide the value of T , which is the time unit at which RadYOLO repeats its operations. Based on the duration of radar signals (burst duration in Table II), we choose $T = 16$ msec. Accordingly, $N = 16 \times 10^4$. $T = 16$ msec is a reasonable choice as it is not too high compared to the shorter radar signals and large enough to capture a significant portion of longer radar signals.

Formation of spectrogram: Next, we perform STFT on the I, Q samples corresponding to a time window. For the STFT, we reshape \mathbf{s} to a matrix, \mathbf{S} , of size $R \times C$. Then, we perform a C point Fast Fourier Transform (FFT) on each of the rows of \mathbf{S} and obtain a new complex matrix \mathbf{F} , which has the same dimension as \mathbf{S} . Finally, we take the logarithm of each element of \mathbf{F} and multiply with 20 to obtain the spectrogram, \mathbf{X}_u . The columns of \mathbf{X}_u represent the different frequency bins, and the rows correspond to the different short terms (we will use the phrase ‘time slots’ to imply the short terms) in our STFT. There is no temporal overlap of the different time slots in our STFT, and we use rectangular windowing in our FFTs.

Dimensions of spectrogram: Since we have fixed the value of T (in turn, N), finding the dimensions of \mathbf{S} requires fixing either R or C . Based on the guidelines for selecting C in [3], we use C such that each of the rows in \mathbf{S} corresponds to a time duration of $1.624 \mu\text{sec}$. The intuitive reasoning behind using a very small time duration for the rows is that the radar pulses are of very short duration, whereas noise or interference is not. Hence, a longer time duration for a row would not increase the amount of radar energy, whereas the amount of energy from non-radar signals would increase significantly and hamper our chances of detecting radar. Selecting the time duration of a row to be $1.624 \mu\text{sec}$ implies $C = 1.624 \times 10^{-6} \times B = 1.624 \times 10^{-6} \times 10 \times 10^6 = 16.24$. Since C must be an integer, we use $C = 16$. Consequently, R becomes $\frac{N}{16} = 10^4$. This implies the number of rows in \mathbf{X}_u is huge and much higher than the number of columns in \mathbf{X}_u .

Compression of spectrogram: To deal with the large number of rows in \mathbf{X}_u , we use a compression method. We reshape \mathbf{X}_u

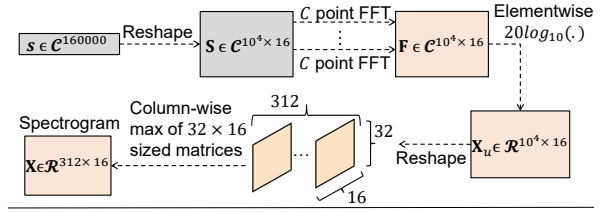


Fig. 2: Operations inside the spectrogram preprocessing block.

of size $(10^4 \times 16)$ to $(312 \times 32 \times 16)$, as shown in Fig. 2. \mathbf{X}_u can be seen as 312 matrices, each of size (32×16) . Next, we compress each of these (32×16) sized matrices to vectors of size 16 by selecting the column-wise maximum for each column. This way, we obtain a new matrix \mathbf{X} of size (312×16) . Fig. 3 shows \mathbf{X} for a set of realizations of the five different types of radar signals listed in Table II. Compression of the spectrogram helps the RadYOLO block in several ways, as explained in next section. In spectrogram compression, we collapse 32 consecutive rows, which correspond to $32 \times 1.624 \approx 52 \mu\text{secs}$, to a single row. Referring to the inter-pulse interval column in Table II, we see the inter-pulse interval of all the radar types is much higher than $52 \mu\text{sec}$. Hence, the ON-OFF patterns created by radar on the spectrograms are not lost by the compression. Additionally, since we assume that the ON time of interference signals is at least 1 msec, our compression technique would not make the interference signal patterns look like radar signal patterns and impact the detectability of radar.

B. RadYOLO

The input to this block is the spectrogram, \mathbf{X} , obtained after spectrogram preprocessing. The core idea of this block is to pass \mathbf{X} through a CNN and apply an object detection algorithm based on YOLO [5] for jointly making radar and interference detection decisions and estimating their parameters. However, using the YOLO framework for signal parameter estimation is challenging. We develop several strategies to deal with these challenges, as described throughout this section.

Definition of objects: We formulate the object detection task as shown in Fig. 4. We take the ambitious step of treating each radar pulse as an object. This way, the number of detected objects can estimate the number of radar pulses, and their separation can estimate the radar pulse interval. Additionally, the height and width of the detected objects can estimate the radar pulse width and bandwidth, respectively. Finally, the x parameter (see Fig. 4(a)) of the detected objects can estimate the radar center frequency. However, as we consider the presence of interference, we must not confuse the interference signals as radar objects. Hence, we treat radar and interference as objects belonging to different classes, as shown in Fig. 4(b). This enables us to detect radar and interference signals simultaneously. Similar to the radar pulses, we define each interference ON duration as an objects (see Fig. 4(b)). Using the detected interference objects, we can estimate their ON times, center frequency, and bandwidth, similarly as described for radar objects.

Object detection framework: Now we explain the object detection framework in RadYOLO. We divide each spectrogram

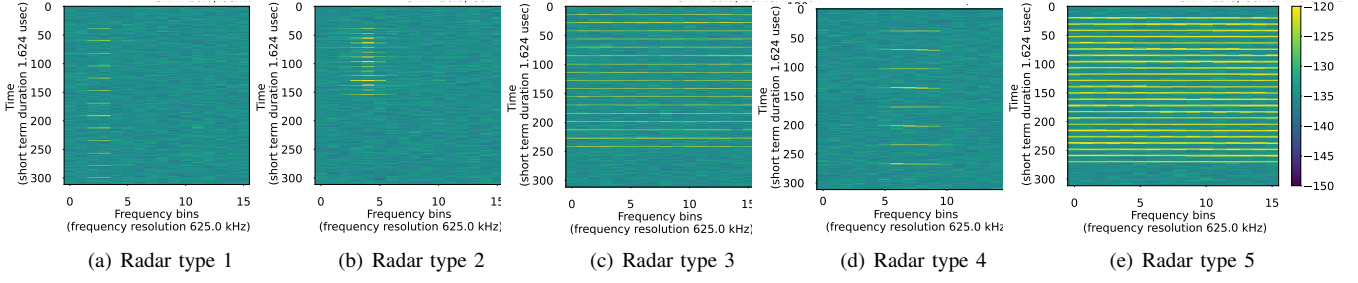


Fig. 3: Example spectrograms of five different radar (20 dB SNR) types after spectrogram preprocessing. No interference signal is present in these examples.

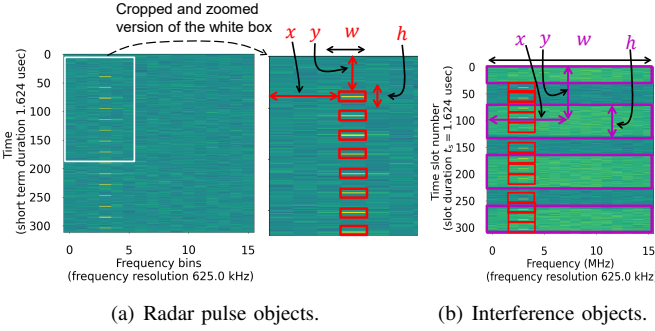


Fig. 4: Definition of radar (red), interference (magenta) objects in RadYOLO.

in a grid of size $K_C \times 1$ (can be visualized as a set of K_C grid cells stacked vertically). The number of grid cells along the frequency axis is 1 because, based on our system model, we do not anticipate multiple signals with nonoverlapping bands on the same spectrogram. Then for each grid cell, we define a bounding box, $(x_i, y_i, w_i, h_i); i = 1, \dots, K_C$, that specifies the location of the object within that grid cell. An object is associated with a grid cell if that object's center lies within the grid cell. The size of an object can be bigger than the size of a grid cell. However, not every grid cell contains an object. Hence, for every bounding box, we define confidence, $c_i; i = 1, \dots, K_C$ (as we use one bounding box per grid cell), which defines the confidence that an object is present in that box. Finally, we must associate the objects with classes. For each grid cell, we use two probabilities, $(p_i^R, p_i^I); i = 1, \dots, K_C$, that are the probabilities that the object in grid cell i belongs to the radar class or interference class, respectively. These probabilities are conditioned on the presence of an object in grid cell i . Note that, with our formulation, we can have only one object per grid cell. Thus, at most, one element of (p_i^R, p_i^I) is non-zero for grid cell i . However, that does not deter us from multi-class classification (detecting both radar and interference on the same spectrogram) as long as all the radar and interference objects do not share the same grid cells. To avoid such undesired situations, we must choose the value of K_C carefully. The choice of K_C is also impacted by the fact that we want different radar pulses/objects to fall in different grid cells so that we can detect them individually. Based on the above factors, we choose K_C to be 32. This choice of K_C implies each of the grid cells corresponds to a duration of $T/K_C = 16/32 = 0.5$ msec, which is comparable to the lowest inter-pulse interval of the different radar types (refer to the Inter-pulse interval column in Table II). Hence, different radar objects will fall in different grid cells with a high probability. Additionally, since the interference signals'

ON time is at least 1 msec, the choice of $K_C = 32$ implies that different interference objects will be in different grid cells, and, with high probability, there will be some grid cells that contain only radar objects. This will improve our chances of detecting radar signals even in interference. Finally, since the number of interference objects on a spectrogram is, in general, smaller than the number of radar objects (see Fig. 4(b)), we associate a grid cell with interference if both radar and interference objects share the grid cell. This will reduce the chances of missing the interference signal altogether.

Training procedure: Based on the above description, we must train the CNN in RadYOLO so that it can predict $(p_i^R, p_i^I, x_i, y_i, w_i, h_i, c_i)$ for each of the K_C grid cells. Thus, for each input spectrogram, the output of the CNN is of size $K_C \times 7 = 32 \times 7$. During training, we minimize the following loss function using the Adam optimizer [23].

$$\begin{aligned}
 \mathcal{L}_Y = & \lambda_{coord} \sum_{b \in \mathcal{B}} \sum_{i=1}^{K_C} \mathbf{1}_{b,i}^{obj} [(x_{b,i} - \hat{x}_{b,i})^2 + (y_{b,i} - \hat{y}_{b,i})^2] \\
 & + \lambda_{coord} \sum_{b \in \mathcal{B}} \sum_{i=1}^{K_C} \mathbf{1}_{b,i}^{obj} \left[\left(\sqrt{w_{b,i}} - \sqrt{\hat{w}_{b,i}} \right)^2 \right. \\
 & \quad \left. + \left(\sqrt{h_{b,i}} - \sqrt{\hat{h}_{b,i}} \right)^2 \right] \\
 & + \lambda_{obj} \sum_{b \in \mathcal{B}} \sum_{i=1}^{K_C} \mathbf{1}_{b,i}^{obj} (c_{b,i} \times \text{IOU}_{b,i} - \hat{c}_{b,i})^2 \\
 & + \lambda_{nobj} \sum_{b \in \mathcal{B}} \sum_{i=1}^{K_C} \mathbf{1}_{b,i}^{nobj} (c_{b,i} \times \text{IOU}_{b,i} - \hat{c}_{b,i})^2 \\
 & + \lambda_{class} \sum_{b \in \mathcal{B}} \sum_{i=1}^{K_C} \sum_{j \in \{R,I\}} \mathbf{1}_{b,i}^{obj} (p_{b,i}^j - \hat{p}_{b,i}^j)^2
 \end{aligned} \tag{1}$$

where b denotes an example belonging to a batch \mathcal{B} , $\mathbf{1}$ denotes an indicator function, and λ_{coord} , λ_{obj} , λ_{nobj} , and λ_{class} are hyperparameters. $\text{IOU}_{b,i}$ is the intersection over union (IOU) of the predicted bounding box and ground truth bounding box for grid cell i of training example b . IOU is defined as the ratio of intersection and union of the predicted bounding box and true bounding box, respectively. IOU represents the quality of localization of an object on the spectrogram.

An important thing to note in (1) is that the ground truth confidence score, $c_{b,i}$, is multiplied by $\text{IOU}_{b,i}$ before it is compared to the predicted confidence $\hat{c}_{b,i}$. This way, the CNN is trained to output high confidence in predicting the presence of an object only when the IOU of the predicted bounding box is

high. However, this creates a challenging problem in our object detection formulation. Since, in our formulation, individual radar pulses are treated as an object, the radar objects are very small with respect to the spectrogram. Consequently, a small localization error for a radar object can result in a very low IOU. If the IOU of the predicted bounding boxes for the radar objects is always low, the network will not be incentivized to predict high confidence, $\hat{c}_{i,b}$, for the radar objects (see (1)). In such cases, it would be difficult for the trained CNN to differentiate between radar objects and background.

To deal with this challenge, we use three strategies. The first strategy is the spectrogram compression, described in Section III-A, which increases the radar objects' size compared to the spectrogram's size. Second, we penalize localization errors (first two terms in (1)) higher than the other terms such that the IOU of the predicted bounding boxes improves. This is done via choosing λ_{coord} to be higher than other hyperparameters. At the same time, we also use a higher value of λ_{obj} such that the predicted confidence is further reduced when no object is present. This way, we aim to have high confidence for radar objects and low confidence for background and, in turn, better distinguishability between radar objects and background. However, using a high value of λ_{coord} causes overfitting. I.e., the localization error is low on the training dataset but not on the validation set. Hence, we carefully choose the values of λ_{coord} and λ_{obj} via cross-validation such that overfitting does not happen during training. Our third strategy is slightly modifying the loss function in (1). Specifically, we modify the definition of IOU as the following:

$$\text{IOU}_{b,i} = \begin{cases} \text{IOU}_{b,i} + 0.5 & \text{if } h_{b,i} < 2\% \text{ of spectrogram height} \\ \text{IOU}_{b,i} & \text{o.w.} \end{cases} \quad (2)$$

From Table II, we can see that the maximum possible radar pulse width is $100 \mu\text{sec}$, which is less than 1% of $T = 16 \text{ msec}$; the duration (height) of the spectrograms. Hence, whenever the true height of an object is less than 2% of the spectrogram height, we provide a boost of 0.5 to the IOU. The value of the boost parameter is chosen to be 0.5 via cross-validation. It is important to note that we must use the second and third strategies simultaneously. If we only use the second strategy while avoiding overfitting, we will not have sufficient confidence in detecting the radar objects. On the other hand, if we only use the third strategy, the network will not learn to perform accurate localization of radar objects. Finally, the interference objects are not affected by the challenge of small objects as they are much larger than the radar objects. Hence, our IOU modification does not affect interference objects as they do not fulfill the criteria in (2).

After training, we extract the following statistical parameters used in the prediction phase.

$c_{R,O}^{max}$: We pass all training examples through the trained CNN. For a training example b , we note the predicted radar confidence score $\hat{c}_{b,i}^R = \hat{c}_{b,i} \times \hat{p}_i^R$ for each of the cells, i , where radar objects are present (based on ground truth). Then, for that training example, we compute $\hat{c}_{b,max}^R = \max_i \hat{c}_{b,i}^R$. Next, we form a set, $C_{R,O}^{max}$, that contains $\hat{c}_{b,max}^R$, for all the training

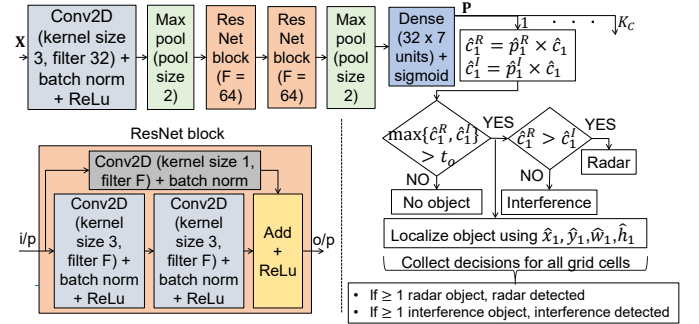


Fig. 5: CNN used in RadYOLO, along with the prediction procedure (shown for grid cell 1, but used for all K_C grid cells.)

examples where radar was present. Finally, we compute $c_{R,O}^{max}$ as the 10th percentile of the set of values in $C_{R,O}^{max}$. Essentially, $c_{R,O}^{max}$ indicates the confidence of the trained model in detecting radar objects.

$c_{R,O}^{min}$: For computing $c_{R,O}^{min}$, we use the same procedure as $c_{R,O}^{max}$, but for each training example we compute $\hat{c}_{b,min}^R = \min_i \hat{c}_{b,i}^R$, instead of $\hat{c}_{b,max}^R = \max_i \hat{c}_{b,i}^R$.

$c_{I,O}^{max}$: We compute this using the same procedure as $c_{R,O}^{max}$, but only for interference objects. $c_{I,O}^{max}$ indicates the confidence of the trained model in detecting interference objects.

$c_{I,O}^{min}$: We compute this using the same procedure as $c_{R,O}^{min}$, but only consider interference objects.

$c_{B,NO}^{max}$: For a training example b , we note the predicted confidence in background $\hat{c}_{b,i}^B = \hat{c}_{b,i} \times [1 - (\hat{p}_i^R + \hat{p}_i^I)]$ for each of the cells, i , where no object is present. Then, for that training example, we compute $\hat{c}_{b,max}^B = \max_i \hat{c}_{b,i}^B$. Next, we form a set, $C_{B,NO}^{max}$, that contains $\hat{c}_{b,max}^B$, for all the training examples where at least one grid cell is present with no object. Finally, we compute $c_{B,NO}^{max}$ as the 95th percentile of the set of values in $C_{B,NO}^{max}$. $c_{B,NO}^{max}$ indicates the false object detection confidence of the trained model when no object is present.

Prediction procedure: The predictions in RadYOLO are made as shown in Fig. 5, which also shows the architecture of our CNN in RadYOLO. We select this architecture based on experimentation. Importantly, the compression method in Section III-A simplifies the CNN architecture by reducing the size of the input spectrogram. The CNN takes \mathbf{X} as the input and produces as output $\mathbf{P} \in \mathcal{R}^{K_C \times 7}$ which consists of $(\hat{p}_i^R, \hat{p}_i^I, \hat{x}_i, \hat{y}_i, \hat{w}_i, \hat{h}_i, \hat{c}_i)$ for each of the $K_C = 32$ cells. First, we multiply \hat{c}_i with \hat{p}_i^R and \hat{p}_i^I to get the class-specific confidence scores, $\hat{c}_i^R = \hat{p}_i^R \times \hat{c}_i$ and $\hat{c}_i^I = \hat{p}_i^I \times \hat{c}_i$, for each of the grid cells. As mentioned before, \hat{p}_i^R represents $\text{Pr}[\text{radar}|\text{object is present}]$ for grid cell i , and \hat{c}_i represents the confidence that an object is present in grid cell i . Hence, \hat{c}_i^R represents the probability of a radar object's presence in grid cell i . Similarly, \hat{c}_i^I represents the probability of an interference object's presence in grid cell i . Next, we find the maximum of \hat{c}_i^R and \hat{c}_i^I and compare it with a threshold, t_o . If $\max\{\hat{c}_i^R, \hat{c}_i^I\} \geq t_o$, we predict the presence of an object in grid cell i . If the presence of an object is predicted, we associate that object with the radar class if $\hat{c}_i^R > \hat{c}_i^I$; otherwise, we associate the object with the interference class. If an object is detected for grid cell i , we estimate its location using $\hat{x}_i, \hat{y}_i, \hat{w}_i, \hat{h}_i$. For a test spectrogram, b , if a radar object is detected in any grid cell, we decide the presence of radar

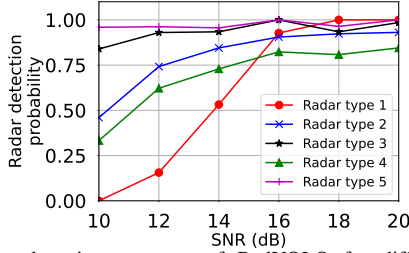


Fig. 6: Radar detection accuracy of RadYOLO for different SNR. No interference is present, and false positive rate is $\approx 0\%$.

signal in example *b*. In such cases, we estimate the radar signal parameters using all the grid cells where radar objects have been detected. Let us denote those grid cells as the set \mathcal{K}_C^R . We estimate the number of radar pulses as $|\mathcal{K}_C^R|$, the center frequency as the mean of $\hat{x}_i; i \in \mathcal{K}_C^R$, the bandwidth of the radar signal as $\cup_i \hat{w}_i; i \in \mathcal{K}_C^R$, the pulse width as the minimum of $\hat{h}_i; i \in \mathcal{K}_C^R$, the pulse interval as the minimum difference between any pair of $\hat{y}_i; i \in \mathcal{K}_C^R$. Similarly, if an interference object is detected for any of the cells in test example *b*, we decide the presence of interference. The interference signal parameters can be estimated using the same procedure as described above for radar signals. For interference signals, we care about center frequency (mean of \hat{x}_i), bandwidth ($\cup_i \hat{w}_i$), and ON times ($\cup_i \hat{y}_i$ and the associated \hat{h}_i), where i runs over the grid cells where an interference object has been detected.

Selection of threshold, t_o : In the prediction procedure, the threshold t_o plays a vital role in deciding whether an object is present. We carefully choose t_o to be $\max\{c_{B,NO}^{max}, \min\{c_{R,O}^{max}, c_{I,O}^{max}\}\}$ and our choice is justified below. As defined earlier, $c_{R,O}^{max}$ and $c_{I,O}^{max}$ are the confidence of the trained model in detecting radar and interference objects, respectively. Thus by choosing t_o to be $\min\{c_{R,O}^{max}, c_{I,O}^{max}\}$, we declare the presence of an object only when the predicted confidence of the trained model is high enough for our target objects. However, we must also ensure that t_o is higher than $c_{B,NO}^{max}$ (false object detection confidence of the trained model when no object is present) to minimize the number of false detection of objects. Hence, instead of using $t_o = \min\{c_{R,O}^{max}, c_{I,O}^{max}\}$, we use $t_o = \max\{c_{B,NO}^{max}, \min\{c_{R,O}^{max}, c_{I,O}^{max}\}\}$.

Capabilities of RadYOLO: The description of RadYOLO explains that it has several capabilities that we aimed for. Recall from Section I that one of our primary goals is to detect low SNR radar signals. In Section III-A, we chose the number of frequency bins in the spectrograms carefully to improve the detectability of radar signals. However, our experiments suggest that such a measure may not be sufficient for low SNR radar signals. Fig. 6 shows the radar detection capability of RadYOLO for different radar SNR. The details of our experiments are presented later in Section IV. We see from Fig. 6 that as radar SNR reduces below 20 dB, the detectability of radar types 1, 2, and 4 is significantly degraded. To tackle this limitation of RadYOLO, we develop another strategy (the second flow in Fig. 1) described in the following two sections.

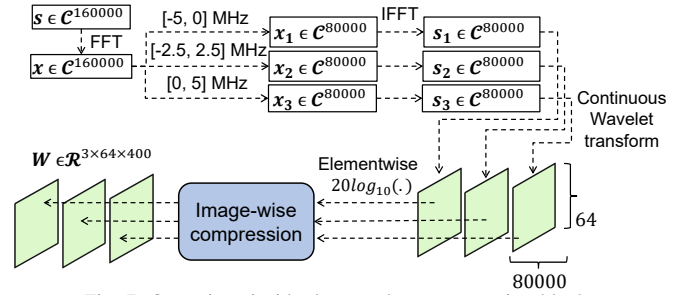


Fig. 7: Operations inside the wavelet preprocessing block.

C. Wavelet Preprocessing

Intuition: The idea of this block is to mimic the operation of matched filtering for improving radar SNR and, thus, its detectability. However, since the detector has no priori knowledge of the radar signal parameters, we design the steps in this block to overcome this problem. The input to this block is the same as the spectrogram preprocessing block, specifically the complex vector s that comprises of the I, Q values. The operations in this block are shown in Fig. 7.

Methods based on matched filtering do not take care of interference. Hence, we take three measures to reduce the impact of interference in the second flow of RadYOLOLet. Out of the three, one is explained in this section, and the remaining two are in the following section.

Filtering: The purpose of this step is the following. From Fig. 6, we see that RadYOLO's main limitation is with radar types 1, 2, and 4. Both radar types 1 and 2 have a fixed bandwidth of 1.6 MHz, and most of RadYOLO's misdetections for radar type 4 are for lower chirp width. Hence, we use the filtering step to look at smaller sub-bands where that radar signal may reside and possibly improve the radar SNR in these sub-bands compared to the whole monitored band. We select the subbands to be overlapped as we do not know the radar center frequency.

Another objective of the filtering step is to contrast radar signals from interference, which is our first measure to deal with interference in the second flow of RadYOLOLet. Recall that the interference signals in our considered system model occupy the whole 10 MHz monitoring band. In contrast, radar types 1, 2, and 4 (main focus of RadYOLOLet's second flow based on Fig. 6) occupy smaller bands. Hence, the sub-bands resulting from the filtering step will have dissimilar patterns on different subbands for radar signals but not for interference.

Now, we present the details of the filtering procedure. First, we perform N point FFT on s to get a complex vector x . Next, we perform rectangular windowing on x to get three different complex vectors x_1 , x_2 , and x_3 . x_1 , x_2 , and x_3 are the frequency domain representation of s over -5 to 0 MHz, -2.5 to 2.5 MHz, and 0 to 5 MHz, respectively, assuming that the sensor's monitoring band is -5 to 5 MHz. Then, we perform IFFT on x_1 , x_2 , and x_3 to obtain s_1 , s_2 , and s_3 , respectively. Essentially, s_1 , s_2 , and s_3 represent the bandpass filtered time domain signals of the original time domain signal s . From the above description, we can see that the complexity of our filtering step increases with the monitoring bandwidth, B . For this reason, using $B = 10$ MHz is convenient for RadYOLOLet as pointed out in Section II.

Wavelet transform: Next, for each bandpass-filtered signal, we perform a CWT, which can be thought of as an equivalent of time-lagged correlation (convolution) of the signal and the filter impulse response. Since we do not know the ideal filter impulse response, we need to find a suitable mother Wavelet function that can approximate the filter impulse response. Additionally, since we do not know the radar signal frequency, the transform must be computed for different frequencies, i.e., for different scale parameters in the Wavelet transform. Now, we explain our Wavelet transform procedure for s_i , which is repeated for $i = 1, 2, 3$.

In CWT, first, we select a mother wavelet function, $\Psi(t)$. Then, we correlate $s_i(t)$ with $\Psi(\frac{t-\delta}{s})$ for different values of δ and s , represented by the following equation [24]:

$$\mathbf{W}_i^u(\delta, s) = \frac{1}{\sqrt{|s|}} \int_{-\infty}^{\infty} s_i(t) \Psi^*\left(\frac{t-\delta}{s}\right) dt \quad (3)$$

where δ is the time lag parameter and s is the scale factor. Lower values of s correspond to compressed versions of the mother wavelet and extract high-frequency information. Higher values of s correspond to expanded versions of the mother wavelet and extract low-frequency information. Since \mathbf{W}_i^u has two parameters, the output of the CWT can be viewed as a matrix of size $L \times S$, where the rows correspond to different lag parameters and the columns correspond to different scale parameters. We leverage this structure of \mathbf{W}_i^u in the Wavelet-CNN block of RadYOLOLet. We investigate the suitability of various mother Wavelet functions and choose the complex Morlet function, given below [6], based on its similarity with radar pulse shapes.

$$\Psi(t) = \frac{1}{\sigma\sqrt{2\pi}} \exp\left[-\frac{1}{2}\left(\frac{t}{\sigma}\right)^2\right] \exp(j2\pi f_0 t) \quad (4)$$

Here σ controls the bandwidth of $\Psi(t)$ and f_0 controls its frequency. (4) represents a complex exponential with a Gaussian envelope. In RadYOLOLet we use $f_0 = 10$ MHz and σ such that the bandwidth of $\Psi(t)$ is 1.5 MHz. Our choices of f_0 and σ are based on the sensor's monitoring bandwidth, B , and radar bandwidth (primarily type 1 and 2).

Dimensions of \mathbf{W}_i^u : The size of \mathbf{W}_i^u is $L \times S$. Since the size of s_i is 80000 we use 80000 different lag parameters in CWT. Hence, we have $L = 80000$. For the scale parameter, we use 64 different values that are uniformly spaced in logarithmic scale in the range $[\log_{10} 0.5, \log_{10} 64]$, which covers the frequencies relevant to our sensor. Thus, we have $S = 64$.

Compression of \mathbf{W}_i^u : As mentioned before, the matrices \mathbf{W}_i^u ; $i = 1, 2, 3$ are fed to a CNN. However, with \mathbf{W}_i^u having a dimension of 80000×64 complicates the design of the CNN architecture. Hence, we apply a compression technique on \mathbf{W}_i^u ; $i = 1, 2, 3$. This compression strategy, denoted as 'Imagewise compression' in Fig. 7, is similar to the compression technique described in Section III-A. Specifically, we reshape \mathbf{W}_i^u of size 80000×64 to $400 \times 200 \times 64$. Then for each of the 200×64 matrices, we retain the column-wise maximum value, resulting in a compressed version of \mathbf{W}_i^u . Let us denote the compressed version of \mathbf{W}_i^u as $\mathbf{W}_i \in \mathcal{R}^{400 \times 64}$. For a particular scale, collapsing 200 consecutive values along the time lag dimension in \mathbf{W}_i^u can be justified in a similar

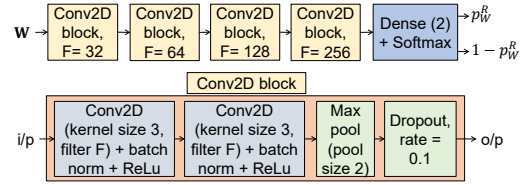


Fig. 8: Neural network architecture of Wavelet-CNN.

manner as done in the context of \mathbf{X}_u . 200 consecutive values along the time lag dimension correspond to $200 \times 0.1\mu\text{sec}$ (inter-sample duration) = $20\mu\text{sec}$, which is much smaller than the radar inter-pulse intervals (refer to Table II).

D. Wavelet-CNN

As discussed in the previous section, the Wavelet preprocessing block tries to mimic the operation of matched filtering. Since the filter impulse response is unknown, we perform the computation in (4) for different values of s . However, we still need to make the detection decision after the approximated matched filtering step. Based on the computed Wavelet transforms, we decide whether a radar signal is present or not. For that, we use a CNN as described next.

The input to Wavelet-CNN is the tensor $\mathbf{W} = [\mathbf{W}_1, \mathbf{W}_2, \mathbf{W}_3]$, whose dimension is $3 \times 400 \times 64$, as shown in Fig. 8. The matrices in \mathbf{W} are similar to the spectrograms discussed in Section III-A. However, the primary difference is that STFTs can represent high resolution in either time or frequency, whereas the matrices in \mathbf{W} (the CWTs) represent high-resolution information in both time and frequency domains. Hence we use \mathbf{W} as the input features to Wavelet-CNN. The neural network acts as a function that performs the following mapping: $\mathcal{F} : \mathcal{R}^{3 \times 400 \times 64} \rightarrow \mathcal{R}^2$, where the input to \mathcal{F} is \mathbf{W} and output is the tuple $(\hat{p}_W^R, 1 - \hat{p}_W^R)$. Here \hat{p}_W^R is the predicted probability of the presence of radar signal. Clearly, \mathcal{F} acts as a binary classifier.

Training procedure: During training, we learn the function \mathcal{F} by minimizing the binary cross-entropy loss function, $\mathcal{L}_W = \sum_{b \in \mathcal{B}} p_{W,b}^R \times \log_2(\hat{p}_{W,b}^R) + (1 - p_{W,b}^R) \log_2(1 - \hat{p}_{W,b}^R)$, using the Adam optimizer. $p_{W,b}^R$ and $\hat{p}_{W,b}^R$ are the true and predicted probabilities of the presence of radar in training example b . After training, we extract the following parameter for the prediction phase.

$p_W^{R,true}$: We pass all the training examples through the trained CNN. We note the predicted radar probability $\hat{p}_{W,b}^R$ for all the examples where radar is present (based on ground truth) and form the set $\mathcal{P}_W^{R,true}$. Finally, we find the g^{th} percentile of $\mathcal{P}_W^{R,true}$ and denote it as $p_W^{R,true}$.

Prediction procedure: During prediction, we pass the input tensor \mathbf{W}_b through the trained CNN, \mathcal{F} and note the predicted radar probability, $p_{W,b}^R$. Then, we compare $p_{W,b}^R$ to a threshold, t_w , and declare the presence of radar only if $p_{W,b}^R \geq t_w$. We select the threshold as $p_W^{R,true}$. Instead of just declaring the presence of radar if $p_{W,b}^R \geq 0.5$, we use the thresholding operation because of the following reason. Since we do not train Wavelet-CNN to differentiate between radar and interference, the network may predict $p_{W,b}^R$ to be greater than 0.5, but not necessarily very high, when only the interference is present. In such cases, we will have false

alarms. Hence, we must choose a non-zero but small value of g in the definition of $p_W^{R,true}$. This is our second measure for tackling interference in RadYOLOLet’s second flow. The third measure is the following.

We assume that the sensor is aware of the interference signal’s center frequency and introduce a slight frequency offset Δ_{CF} at the sensor with respect to the interference signal. The center frequency offset will introduce distortions in the digitally modulated interference signals and appear as noise to the subsequent signal processing steps.

Parameter estimation: Wavelet-CNN cannot estimate signal parameters. We develop a strategy to partially address this limitation. Our strategy is to reuse the neural network output of RadYOLO, \mathbf{P} , but apply a different post-processing technique. Recall from Section III-B that during prediction, RadYOLO first decides whether an object is present or not. Then, it performs object localization ($\hat{x}_i, \hat{y}_i, \hat{w}_i, \hat{h}_i$) only if an object has been detected. Once we are into the second flow of RadYOLOLet, it is evident that no radar object was detected by RadYOLO. However, if Wavelet-CNN predicts the presence of a radar signal, we can override the object detection decision of RadYOLO. Overriding the object detection decision of RadYOLO implies using an object detection threshold, say t_o^w , that is different from t_o (refer to Fig. 5). t_o^w must be lower than t_o ; otherwise, no radar object would be detected, as was the case with RadYOLO in the first place. Note that by using a lower object detection threshold, we are not affecting RadYOLOLet’s radar false alarm rate as the decision regarding the presence of radar has already been made by Wavelet-CNN. However, a very low value for t_o^w may cause many false object detections and adversely affect the radar parameter estimation quality. Based on these factors, we choose t_o^w to be $c_{R,O}^{min}$. Recall from Section 5 that $c_{R,O}^{min}$ considers the minimum confidence of all the radar objects on a spectrogram, whereas $c_{R,O}^{max}$ (used in t_o) considers the maximum. Using t_o^w , we perform the object detection and localization on \mathbf{P} as shown in Fig. 5 with the only difference that the procedure is applied only to radar class as Wavelet-CNN only impacts radar detection.

IV. EVALUATIONS

In this section, first, we describe the datasets and experiments. Next, we present the evaluation metrics and the baseline methods. Finally, we present the evaluation results.

A. Datasets

Radar: For radar signals, we rely on a dataset generated synthetically by NIST [25]. This dataset provides several captures, each of 80 msec, in the form of I, Q values. The captures correspond to a 10 MHz band. Almost half of the captures have no radar signal (receiver noise only), and the remaining ones with radar. Each of the captures containing a radar has at most one radar signal, chosen randomly from the five radar types listed in Table II. The radar parameters are randomly chosen from the ranges specified in Table II. The SNR of the radar signals is chosen randomly from [10, 12, 14, 16, 18, 20] dB, and no interference signal is present in the captures. For

our evaluations, we use 9000 captures with 50:50 split between radar and noise.

Interference: For evaluating RadYOLOLet in interference, we generate several interference datasets. As discussed in Section II, the interference signals are assumed to be downlink signals from a BS. For the following datasets, INR is defined as the ‘average interference-plus-noise to average noise ratio’ over a band of 1 MHz around the interference signal’s center frequency. This is done so that the SINR values can be easily computed and to make the SINR values meaningful. (Recall from Section I that radar SNR values are also defined similarly).

QPSK ON dataset: Using MATLAB, we generate 2000 captures of QPSK signals with a bandwidth of 9.1 MHz and a center frequency offset of $\Delta_{CF} = 0.35$ MHz with respect to the sensor’s center frequency. Each capture is 80 msec, and the QPSK signal is always ON within one capture. The QPSK signal changes at the symbol rate. The INR is randomly chosen from [2, 4, 6, 8, 10] dB across captures but is kept constant within a capture.

QPSK ON-OFF dataset: Similar to QPSK ON dataset but the QPSK signal turns ON for 3 msec and then off for 2 msec. One such ON-OFF pattern is shown in Fig. 4(b).

LTE FDD dataset: Using MATLAB LTE toolbox [26], we generate 2000 captures LTE downlink captures that occupy 50 resource blocks (9 MHz). This dataset’s frequency offset, capture duration, and INR values are similar to other datasets. For this dataset, we use LTE frequency division duplexing (FDD) mode [22], where BSs and UEs use different frequencies.

LTE TDD dataset: This dataset is similar to the above dataset, but we use LTE time division duplexing (TDD) [22], where BSs and UEs use the same band for their transmissions but take turns in multiples of LTE slot duration (1 msec) defined via the uplink/downlink (UL/DL) configurations. For each capture, we randomly choose one of seven possible UL/DL configurations [22].

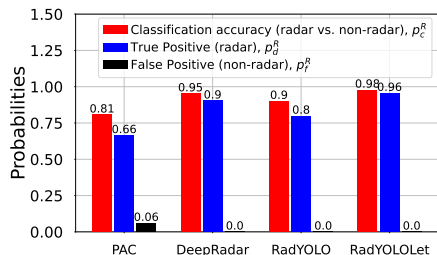
B. Experiments

Using the above datasets, we conduct three experiments.

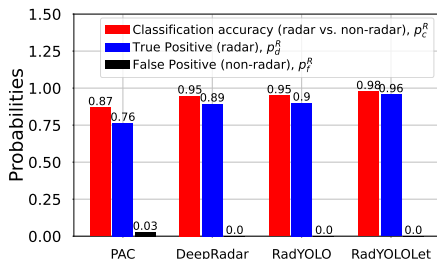
Experiment 1: We create a training dataset of 2500 radar, 2500 AWGN (receiver noise), 2500 interference, and 2500 radar plus interference captures. We randomly select between QPSK ON and QPSK ON-OFF for the interference captures. For the radar plus interference captures, we simply add the I, Q values of radar and interference (randomly chosen between QPSK ON and QPSK ON-OFF) while ensuring that receiver noise is not added twice. For each of the captures, we select a 10 msec long capture from the 80 msec captures in the datasets. The radar and interference start time within the 10 msec capture are randomized. We train different methods (described later in this section), including RadYOLOLet, using these 10,000 examples. For all the deep learning methods, we use the Keras [27] framework. We evaluate the trained models using various metrics (explained later) on the test set. The test set has 4000 examples, almost half radar and the remaining AWGN. Note that the test set has no interference.

TABLE III: Evaluations metrics

Metric	Definition
p_c^R	Binary classification accuracy between radar and non-radar (both with and without interference)
p_d^R	Fraction of examples with radar that is correctly detected; radar true positive rate
p_f^R	Fraction of examples with no radar but falsely detected; radar false positive rate
p_c^I	Binary classification accuracy between interference and non-interference (with and without radar)
p_d^I	Fraction of examples with interference that is correctly detected; interference true positive rate
p_f^I	Fraction of examples without interference but falsely detected; interference false positive rate
b_M^R	Average radar missed bandwidth (for examples where radar is correctly detected and pulse parameters estimated)
b_E^R	Average radar bandwidth estimated in excess (for examples where radar is correctly detected and pulse parameters estimated)
n_P^R	Average percentage of detected radar pulses (for examples where radar is correctly detected and pulse parameters estimated)
e_{PW}^R	Average pulse width absolute error (for examples where radar is correctly detected and pulse parameters estimated)
e_{PI}^R	Average pulse interval estimation absolute error (for examples where radar is correctly detected and pulse parameters estimated)
t_M^I	Average interference missed ON time (for examples where interference is correctly detected and parameters estimated)
t_E^I	Average interference ON time estimated in excess (for examples where interference is correctly detected and parameters estimated)



(a) Experiment 1, AWGN



(b) Experiment 3, AWGN

Fig. 9: Binary classification between radar and non-radar signals, which for these plots is AWGN, for different methods.

Experiments 2A and 2B: We use the models trained in experiment 1, but the test sets are different. For both experiments 2A and 2B, the test set contains 4000 examples, with almost half of them radar plus interference and the remaining interference only. The interference signals are QPSK ON and QPSK ON-OFF for experiments 2A and 2B, respectively.

Experiment 3: This experiment is similar to experiment 1, but in this case, we use the LTE FDD and TDD interference signals for the training instead of QPSK interference.

Experiments 4A and 4B: These experiments are similar to experiments 2A and 2B, but we use the models trained as part of experiment 3. The interference signals are LTE FDD and LTE TDD for experiments 4A and 4B, respectively.

C. Metrics

We evaluate RadYOLOLet and compare it with other methods using the metrics in Table III.

D. Methods for comparison

In this section, we describe the methods that we use to compare RadYOLOLet's performance.

Peak analysis classifier (PAC) [14]: This method computes the following features and uses them for training an SVM-based binary classifier. The features are mean, variance, maximum of the time intervals between the peaks of the amplitude,

and the mean amplitude of the peaks of the captured signal. This method can only distinguish between radar and non-radar signals. Hence, it cannot detect interference signals, and also cannot estimate the signal parameters.

DeepRadar [3]: This method treats all the radar pulses on a spectrogram as a single object and applies YOLO for detecting and localizing those objects. As a result, this method can estimate radar center frequency and bandwidth but cannot estimate the temporal parameters. For a fair and meaningful comparison with RadYOLOLet, we make some modifications in DeepRadar. First, DeepRadar considers 100 MHz monitoring bandwidth and uses multiple grid cells in YOLO along the frequency axis of the spectrograms. However, in this paper, we consider the monitoring bandwidth to be 10 MHz. Accordingly, we use only one grid cell in DeepRadar's YOLO along the frequency axis of the spectrograms. Second, we apply the preprocessing proposed in this paper also to the spectrograms fed to DeepRadar.

RadYOLO: This is simply our proposed scheme, but without using the second flow of Fig. 1.

E. Results

1) *Radar vs. non-radar classification in AWGN:* Using experiments 1 and 3, we compare the classification (radar versus AWGN) accuracy of different methods in Fig. 9. The results are combined for SNR range [10–20] dB and all radar types. We make the following observations.

First, differences in training data lead to different models for the same method. Thus, the performances of PAC and RadYOLO are different for experiments 1 and 3, which have similar test data but different training data. The trained models for experiment 3 perform better than those for experiment 1 because the interference patterns in experiment 3's training data are less obscuring. Specifically, the LTE TDD interference has a lower average ON time (6 msec) due to the different possible UL/DL configurations than the average ON time of QPSK ON-OFF signals (9 msec). RadYOLO is sensitive to interference as it treats interference as a different class, unlike Wavelet-CNN and DeepRadar. The reason for PAC's sensitivity to interference is different. PAC relies on the amplitude peak statistics, which are affected by interference. This figure also shows the robustness of our overall scheme RadYOLOLet as it is unaffected by the differences in the training data. It appears that DeepRadar is also unaffected by the differences in the training data, but subsequent results will show that this is not the case in all experiments.

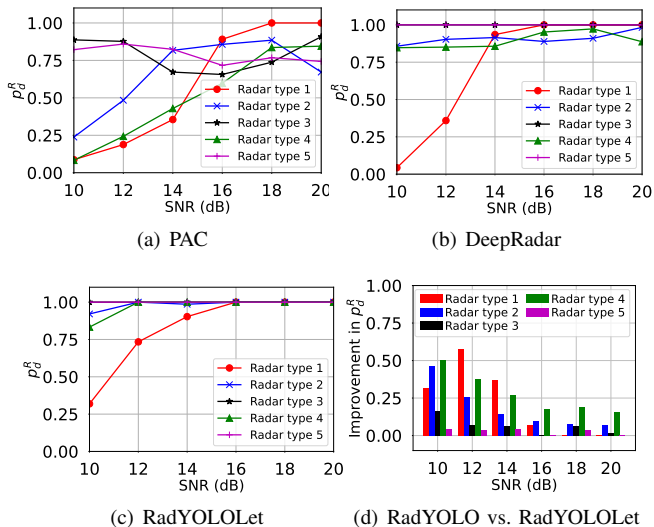


Fig. 10: Comparison of different methods in terms of radar detection accuracy, p_d^R , for fixed AWGN power but varying radar signal power.

Second, for all the metrics considered in Fig. 9, PAC does not perform as well as the other methods, justifying the need for deep learning-based classification in our problem. The handcrafted feature extraction also limits PAC’s pattern recognition capability.

Third, DeepRadar performs better than RadYOLO in Fig. 9(a). This is because our object detection formulation, described in Section III-B, is more complex than that of DeepRadar. We use a complex framework to estimate more signal parameters than DeepRadar. However, the added complexity hurts RadYOLO’s radar detection performance to some extent.

Fourth, although DeepRadar performs better than RadYOLO in experiment 1, our overall method, RadYOLOLet, outperforms all other methods due to the combined use of RadYOLO and Wavelet-CNN. Thus, by combining the benefits of the two flows, RadYOLOLet can achieve both superior classification accuracy and diverse parameter estimation capability.

Fifth, RadYOLO and RadYOLOLet have radar false positive rate below 1% due to careful selection of thresholds, t_o and $p_W^{R,true}$, described in Section III-B and III-D. DeepRadar has low p_f^R as it deals with larger objects, unlike RadYOLO, and is less prone to false object detections.

2) *Radar detection accuracy versus SNR*: Fig. 9 showed the radar true positive rate, p_d^R , combined across all SNR values and all radar types. To gain insights about performance across different SNRs, in Fig. 10, we show different methods’ p_d^R for individual radar types and different values of SNR using the results of experiment 1. Fig. 10 does not show the results for RadYOLO as it was presented before in Section III-B. Hence in Fig. 10(d), we show RadYOLOLet’s improvement in p_d^R over that of RadYOLO. Our primary observations are the following.

First, for all the methods detecting radar type 1 for low SNR becomes difficult. This can be explained using Table II, which shows that the pulse width of radar type 1 is much smaller than others. A lower value of radar pulse width implies that the sensor must detect the radar using less signal energy. We also see that the performance trends corresponding to

different radar types are similar for all the methods. This implies some radar types are inherently more challenging to detect than others. For example, different radar types have different bandwidth. Hence, even for the same per MHz SNR (the way we defined SNR as per CBRS rules), the total SNR can be different for different radar types.

Second, although the p_d^R improvement in RadYOLOLet over DeepRadar is 6% in Fig. 9, we see a more important difference from Fig 10(b), (c). RadYOLOLet can achieve 100% p_d^R for all radar types up to 16 dB SNR. DeepRadar can achieve high p_d^R for all radar types up to 14 dB, but it cannot guarantee 100% p_d^R while ensuring a false positive rate below 1%. RadYOLOLet’s superior performance in low SNR is due to the robustness of Wavelet-CNN and its preprocessing.

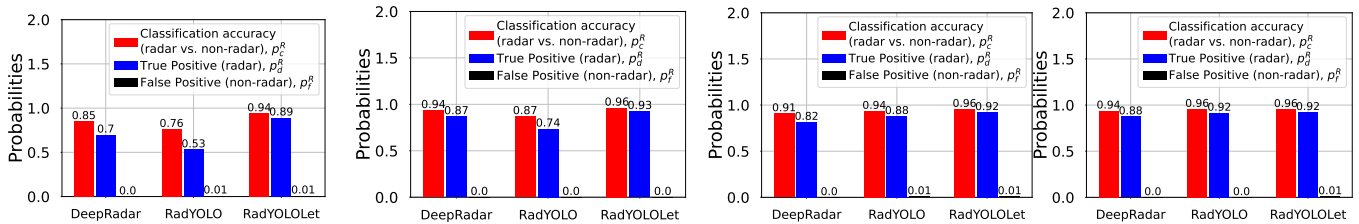
Third, Fig. 10(d) shows that the main p_d^R improvement of RadYOLOLet over RadYOLO is in the low SNR regime, especially for radar types 1, 2, and 4, which is precisely what we aimed for in the second flow of RadYOLOLet.

3) *Radar vs. non-radar classification in interference*: In Fig. 11, we compare the radar versus non-radar classification accuracy for different methods in the presence of different types of interference. The results are combined for SNR range [10-20] dB and INR range [2-10] dB, i.e., SINR range [0-18] dB. Results in Fig. 11(a), 11(b) are obtained using the model trained in experiment 1. Results in Fig. 11(c), 11(d) are obtained using the model trained in experiment 3.

First, we see that for all four experiments, RadYOLOLet has the best performance in terms of p_c^R and p_d^R . This shows that our proposed method can detect radar accurately, even in interference. Importantly, Fig. 11 also shows that RadYOLOLet achieves this high radar detection accuracy while ensuring that the radar false positive rate, p_f^R , is less or equal to 1%. This demonstrates that the measures we took for dealing with interference in Section III-C and III-D are effective.

Second, comparing Fig. 11(a), 11(b), we see that, for all the methods, the classification accuracy, p_c^R , is higher with QPSK ON-OFF interference than QPSK ON interference. The reason is that QPSK ON interference is always ON, making it more difficult to detect the radar signals. On the other hand, QPSK ON-OFF interference turns ON intermittently. A similar observation can be made by comparing Fig. 11(c), 11(d). Fig. 11(c) corresponds to LTE FDD interference, which is always ON, and Fig. 11(d) corresponds to LTE TDD, which is intermittently ON. However, the performance gap between Fig. 11(c), 11(d) is less than that of Fig. 11(a), 11(b). The explanation for the following observation also answers this.

Third, by comparing Fig. 11(a), 11(b) with Fig. 11(c), 11(d) we observe that RadYOLO and DeepRadar perform better with LTE interference than QPSK interference. The reason for that is the following. When RadYOLO and DeepRadar are trained with QPSK interference (refer to experiment 1), their object detection models have some overfitting because of interference. I.e., the models produce high confidence for the detected radar objects based on training data (the confidences influence the object detection thresholds) but the confidence for test radar objects is lower. This primarily affects the test data in experiment 2A, where the test signals have QPSK ON interference. Also, this problem is more prominent for



(a) Expt. 2A, QPSK ON interference (b) Expt. 2B, QPSK ON-OFF interference (c) Expt. 4A, LTE FDD interference (d) Expt. 4B, LTE TDD interference

Fig. 11: Classification between radar and non-radar for different methods. Both radar and non-radar signals have interference on top of the noise floor. Results are combined for SNR range [10-20] dB and INR range [2-10] dB, i.e., SINR range [0-18] dB.

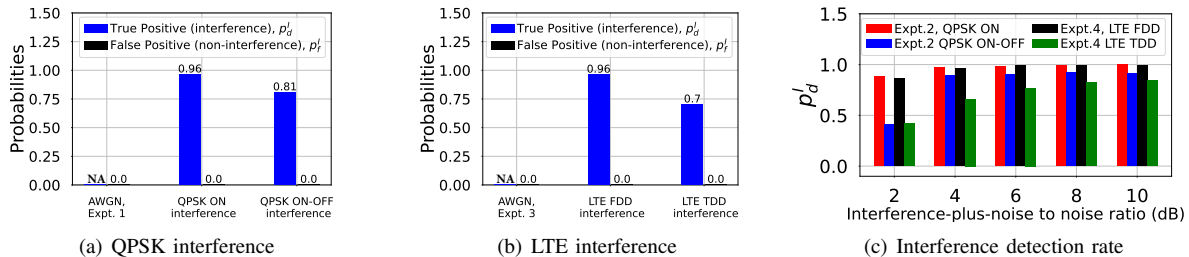


Fig. 12: Classification between interference and non-interference using RadYOLO. The radar SNR and interference INR ranges are the same as in Fig. 11. Fig. 12(c) shows the interference detection rate of RadYOLO for different INR in different experiments.

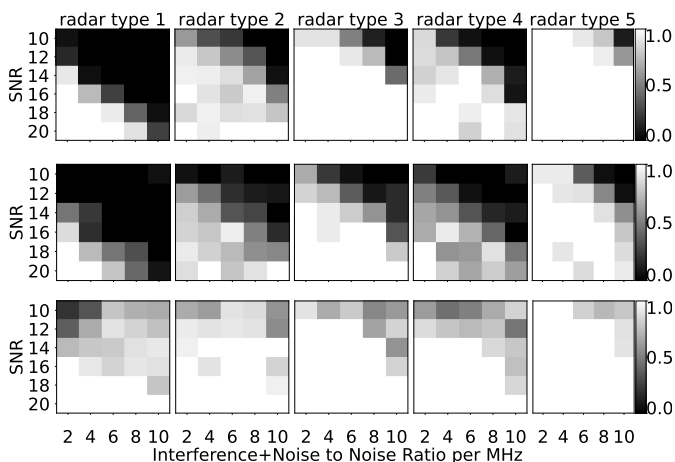


Fig. 13: Radar detection probability, p_d^R , for DeepRadar (top), RadYOLO (middle), and RadYOLOLet (bottom) for experiment 2A.

RadYOLO because of the small radar pulse objects. On the other hand, for the RadYOLO and DeepRadar models trained with LTE interference, this issue is less severe because the interference patterns in the training data are less obscuring, as discussed in Section IV-E1. However, Fig. 11 also reveals that our overall scheme RadYOLOLet is less affected by the above issue because of the use of Wavelet-CNN to aid RadYOLO. Wavelet-CNN does not use an object detection and is less interference-sensitive. Hence, RadYOLOLet has consistent performance across all four cases in Fig. 11.

4) *Interference vs. non-interference classification*: In Fig. 11, we argued that the undetected radar signals in RadYOLO are miss detections, not miss classifications. This is demonstrated in Fig. 12(a) and 12(b), showing that the interference false positive rate is always 0%. Note that the results in Fig. 12 are only for RadYOLO as the other methods cannot classify interference signals. In experiments 1 and 3, we do not have any interference signal in the test set. Hence

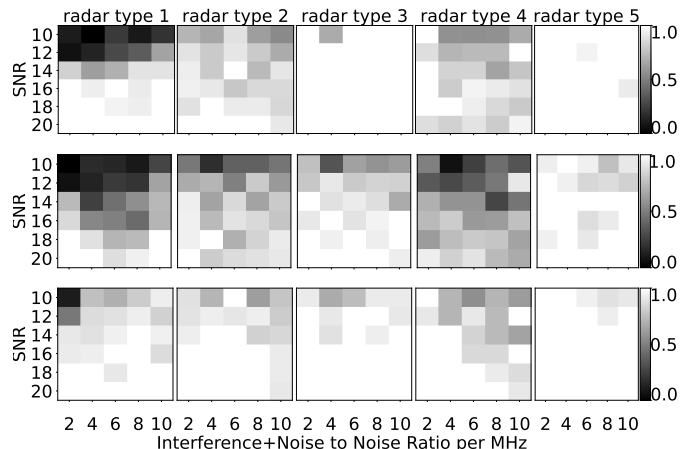


Fig. 14: Radar detection probability, p_d^R , for DeepRadar (top), RadYOLO (middle), and RadYOLOLet (bottom) for experiment 2B.

for these two experiments, we use 'NA' for interference true positive rate, p_d^I . Fig. 12(a) and 12(b) also show that the p_d^I with QPSK ON and LTE FDD interference is very high. However, that is not the case for QPSK ON-OFF and LTE TDD. The reason is interference objects corresponding to QPSK ON and LTE FDD signals are much bigger than that of QPSK ON-OFF and LTE TDD signals. Hence, they are easier to detect with high confidence. Due to similar reasoning, p_d^I for QPSK ON-OFF is higher than that of LTE TDD.

Fig. 12(c) shows the interference detection rate, p_d^I , for different values of INR and different experiments. This figure shows that the interference signals are missed more in the low INR region. This is expected because, at low INR regions, the interference objects are less detectable. Importantly, the missed interference signals are not miss classified as radar as demonstrated by the $\leq 1\%$ radar false positive rate in Fig. 11.

5) *Radar detection performance at different SINR*: Next, we analyze p_d^R for experiments 2A, 2B, 4A, and 4B in Fig. 13, 14, 15, and 16, respectively, for different values SINR and the

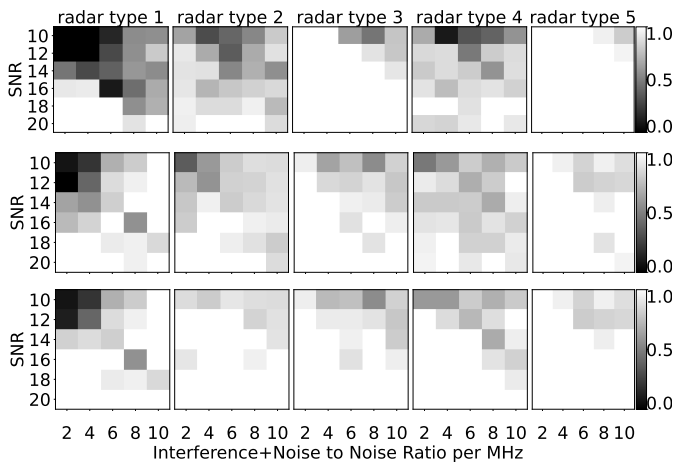


Fig. 15: Radar detection probability, p_d^R , for DeepRadar (top), RadYOLO (middle), and RadYOLOLet (bottom) for experiment 4A.

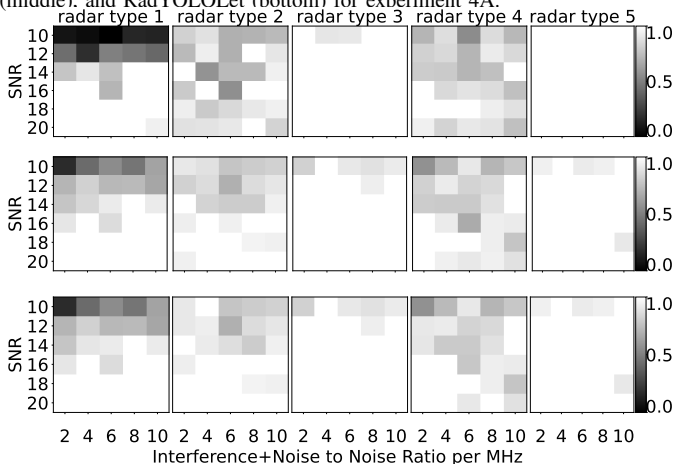


Fig. 16: Radar detection probability, p_d^R , for DeepRadar (top), RadYOLO (middle), and RadYOLOLet (bottom) for experiment 4B.

different radar types. Since we vary both the radar SNR and the interference INR, the results are shown as images where the pixel values are p_d^R , the INR increases along the x-axis, and the SNR increases along the y-axis. The primary observation is that irrespective of the interference type, RadYOLOLet can tolerate up to 4 dB INR and still achieve 100% radar detection accuracy when the radar SNR is fixed at 20 dB. On the other hand, if we fix the INR to be 2 dB, then RadYOLOLet can achieve 100% p_d^R for SNR up to 18 dB. The above two observations suggest that RadYOLOLet can accurately function up to 16 dB radar SINR. This is not achievable by the other two methods. These figures also show that the second flow of RadYOLOLet assists RadYOLO not only in AWGN but also in different types of interference.

6) *Signal parameter estimation*: In Fig. 17, we show the parameter estimation of different methods. Fig. 17(a) is an example estimation of RadYOLO that will help us explain some observations. In Fig. 17, along with RadYOLO and RadYOLOLet, we evaluate DeepRadar for bandwidth estimation but not for the other parameters as DeepRadar cannot estimate them.

First, we see from Fig. 17(b), 17(c) that both in terms of missed and excess bandwidth, DeepRadar performs better than RadYOLO and RadYOLOLet. The difference is marginal in

terms of b_M^R , and all the methods have a low missed bandwidth error. However, b_E^R for RadYOLO and RadYOLOLet is at least 1 MHz higher than that of DeepRadar. This happens because RadYOLO attempts to detect each radar pulse individually and decides the signal bandwidth to be the union of the bandwidth of the individual pulses. As we can see from Fig. 17(a), the bandwidth estimation of individual pulses can be different, leading to a wider estimated bandwidth than the actual. Since RadYOLOLet relies on RadYOLO's bandwidth estimation, it also has the same problem. DeepRadar does not have this problem because it treats all the pulses as a single object. However, this also is a limitation of DeepRadar as it cannot estimate the temporal parameters.

Second, Fig. 17(d) shows that both RadYOLO and RadYOLOLet detect 40-75% of the radar pulses. This shows the difficulty of detecting small radar pulse objects. Even after prioritizing the small objects in the loss function in (1), RadYOLO cannot detect all pulses. However, this is not a major problem as RadYOLOLet does not require detecting all the radar pulses for estimating pulse width and interval as explained in Section III-B. Fig. 17(d) also shows that RadYOLO and RadYOLOLet detect more pulses for the model trained in experiment 3. The reason is the difference in training data in experiments 1 and 3, as explained in the context of Fig. 11. However, a higher n_P^R also increases the possibility of excess bandwidth estimation. Thus, b_E^R for RadYOLO and RadYOLOLet is higher in experiments 4A, 4B as shown in Fig. 17(c).

Third, Fig. 17(e) shows that the pulse width estimation error of RadYOLO is high with respect to the true average radar pulse width. However, Fig. 17(a) shows that the estimated width of the pulses (height of objects on spectrogram) is well aligned with the actual pulses. This incongruence arises from the fact that the radar pulse width is very low, on average 30 μ sec, and the errors are also shown in μ sec, which is difficult to interpret visually from Fig. 17(a). The error in pulse width can be attributed to the difficulty in estimating the extremely small radar pulse width.

Fourth, we see from Fig. 17(f) that the pulse interval errors are lower when the test set contains no interference signal. This happens because in the presence of interference, RadYOLO misses a higher number of pulses, which is reflected by Fig. 17(d). This, in turn, affects the pulse interval estimation, which is the minimum gap between any pair of detected pulses.

Fifth, for almost all the plots in Fig. 17 RadYOLOLet's performance is comparable to that of RadYOLO. While this is expected as RadYOLOLet relies on RadYOLO's estimations, it is important to note that RadYOLOLet's results are based on more test examples than RadYOLO. This is demonstrated via Fig. 17(g), which shows the percentages of test data on which the methods perform successful radar detection and parameter estimation. RadYOLO's detection and estimation percentage is always same as they are done jointly. RadYOLOLet's detection percentage is strictly better than that of RadYOLO as discussed in Fig. 9, 11. RadYOLOLet's estimation percentage is better than that of RadYOLO due to Wavelet-CNN's parameter estimation approach presented in Section III-D. However, as the detections and estimations are decoupled in Wavelet-CNN,

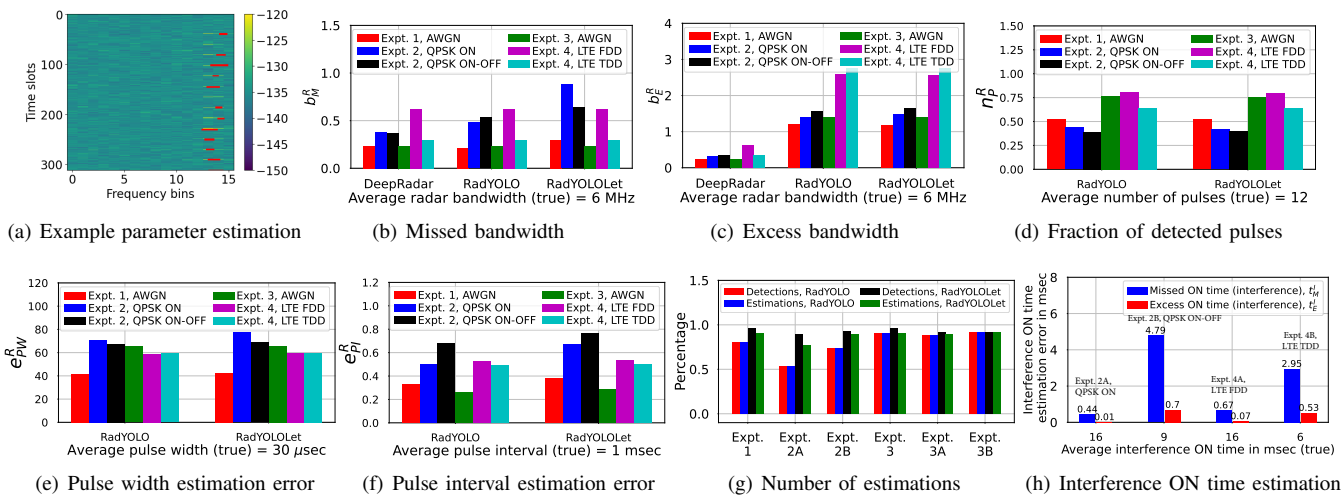


Fig. 17: Signal parameter estimation of different methods. Except for the last one, all other figures are for radar signal parameters.

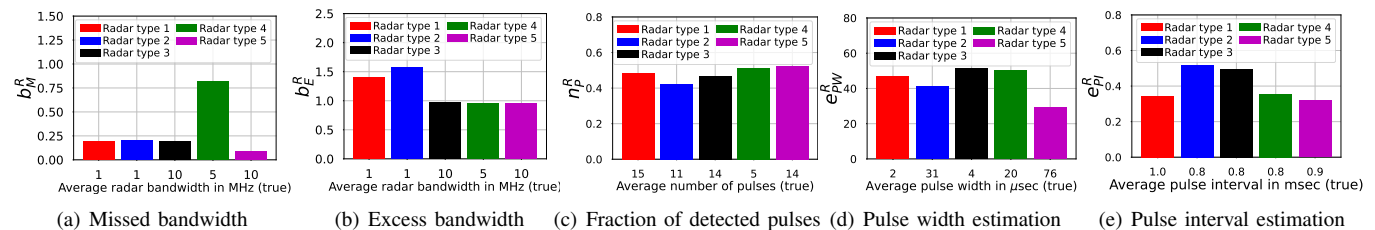


Fig. 18: Radar signal parameter estimation for different types using experiment 1.

its estimation percentage is always lower than its detection percentage.

Fig. 17(h) shows the parameter estimation for interference signals. Recall that Wavelet-CNN cannot improve interference detection and estimation performance compared to RadYOLO. Hence, the results in Fig. 17(h) are for RadYOLO. We see that the ON time estimation errors are very small for experiments 2A, 4A. This is because the interference objects in these experiments have fixed sizes, i.e., lesser uncertainty. On the other hand, the estimation errors are higher for experiments 2B and 4B because the interference objects in these experiments can have unknown locations and sizes. The missed ON time is higher in experiment 2A because the interference objects for QPSK ON-OFF interference are larger than the interference objects for LTE FDD.

F. Radar signal parameter estimation for different types

Fig. 17 shows the results for all radar types combined. To provide more insights, we show RadYOLO's radar parameter estimation for different radar types in Fig. 18. The results in this figure are for experiment 1. The observations from this figure are the following. First, the missed bandwidth is higher for radar type 4 as its bandwidth variability is higher than that of other radar types. Second, the excess bandwidth is higher for radar types 1 and 2 because they are narrower than the other radar types. Third, the pulse width estimation error is lower for radar type 5 as its pulse width is higher than the remaining ones. Fourth, the pulse interval estimation error is relatively higher for radar types 2 and 3. This happens because the number of detected pulses affects the pulse interval estimation. We can see from Fig. 18(c) that the fraction of detected pulses is lower for these two radar types.

V. CONCLUSIONS AND FUTURE WORK

We presented RadYOLOLet, a novel deep-learning-based versatile spectrum sensing method for detecting radar and estimating their parameters. We developed two different CNNs, RadYOLO and Wavelet-CNN, that are the workhorse for RadYOLOLet. Both the CNNs and their inputs and outputs were carefully designed. We thoroughly evaluate RadYOLOLet using a diverse set of experiments. Our evaluations demonstrate the efficacy of RadYOLOLet both in low SNR and low SINR. Specifically, RadYOLOLet can achieve 100% radar detection accuracy to 16 dB SNR, as well as 16 dB SINR, which cannot be guaranteed by other comparable methods.

REFERENCES

- [1] A. W. Clegg *et al.*, "Radar sharing in the us 3 ghz band," in *2022 IEEE Radar Conference*. IEEE, 2022, pp. 1–5.
- [2] "Citizens Broadband Radio Service." *Code of Federal Regulations*, no. Title 47, Part 96, 2016.
- [3] S. Sarkar *et al.*, "Deepradar: A deep-learning-based environmental sensing capability sensor design for cbrs," in *Proceedings of the 27th Annual International Conference on Mobile Computing and Networking*, 2021, pp. 56–68.
- [4] "Requirements for Commercial Operation in the U.S. 3550-3700 MHz Citizens Broadband Radio Service Band," <https://winnf.memberclicks.net/assets/CBRS/WINNF-TS-0112.pdf>.
- [5] J. Redmon, S. Divvala, R. Girshick, and A. Farhadi, "You only look once: Unified, real-time object detection," in *Proceedings of the IEEE conference on computer vision and pattern recognition*, 2016, pp. 779–788.
- [6] J. E. Ball and A. Tolley, "Low snr radar signal detection using the continuous wavelet transform (cwt) and a morlet wavelet," in *2008 IEEE Radar Conference*. IEEE, 2008, pp. 1–6.
- [7] N. Soltani, V. Chaudhary, D. Roy, and K. Chowdhury, "Finding waldo in the cbrs band: Signal detection and localization in the 3.5 ghz spectrum," in *GLOBECOM 2022-2022 IEEE Global Communications Conference*. IEEE, 2022, pp. 4570–4575.

- [8] M. A. Richards, J. Scheer, W. A. Holm, and W. L. Melvin, *Principles of modern radar*. Citeseer, 2010, vol. 1.
- [9] S. A. Vorobyov, "Principles of minimum variance robust adaptive beamforming design," *Signal Processing*, vol. 93, no. 12, pp. 3264–3277, 2013.
- [10] R. Li *et al.*, "Fast ml-assisted interference estimation and suppression for digital phased array radar," in *2022 IEEE International Symposium on Phased Array Systems & Technology (PAST)*. IEEE, 2022, pp. 1–8.
- [11] "Potential Metrics for Assessing the Impact of ESC Sensors and Networks on CBRS Deployments," https://winnf.memberclicks.net/assets/work_products/Reports/WINNF-TR-1015-V1.0.0%20ESC%20Sensor%20Impact%20Technical%20Report.pdf.
- [12] S.-H. Kong, M. Kim, L. M. Hoang, and E. Kim, "Automatic lpi radar waveform recognition using cnn," *Ieee Access*, vol. 6, pp. 4207–4219, 2018.
- [13] A. Selim *et al.*, "Spectrum monitoring for radar bands using deep convolutional neural networks," in *GLOBECOM 2017-2017 IEEE Global Communications Conference*. IEEE, 2017, pp. 1–6.
- [14] R. Caromi, M. Souryal, and W.-B. Yang, "Detection of incumbent radar in the 3.5 GHz CBRS band," in *2018 IEEE Global Conference on Signal and Information Processing (GlobalSIP)*. IEEE, 2018, pp. 241–245.
- [15] W. M. Lees *et al.*, "Deep Learning Classification of 3.5 GHz Band Spectrograms with Applications to Spectrum Sensing," *IEEE Transactions on Cognitive Communications and Networking*, 2019.
- [16] R. Caromi and M. Souryal, "Detection of Incumbent Radar in the 3.5 GHz CBRS Band using Support Vector Machines," in *2019 Sensor Signal Processing for Defence Conference (SSPD)*. IEEE, 2019, pp. 1–5.
- [17] X. Wang, "Electronic radar signal recognition based on wavelet transform and convolution neural network," *Alexandria Engineering Journal*, vol. 61, no. 5, pp. 3559–3569, 2022.
- [18] M. Zheleva *et al.*, "Airview: Unsupervised transmitter detection for next generation spectrum sensing," in *IEEE INFOCOM 2018-IEEE Conference on Computer Communications*. IEEE, 2018, pp. 1673–1681.
- [19] M. Walencykowska and A. Kawalec, "Radar signal recognition using wavelet transform and machine learning," in *2022 23rd International Radar Symposium (IRS)*. IEEE, 2022, pp. 492–495.
- [20] F. H. Sanders, J. E. Carroll, G. A. Sanders, R. L. Sole, J. S. Devereux, and E. F. Drocella, "Procedures for laboratory testing of environmental sensing capability sensor devices," *Technical Memorandum TM*, pp. 18–527, 2017.
- [21] "An Analysis of Aggregate CBRS SAS Data from April 2021 to January 2023," <https://its.ntia.gov/publications/details.aspx?pub=3311>.
- [22] MATLAB, "FDD and TDD Duplexing," <https://www.mathworks.com/help/lte/ug/fdd-and-tdd-duplexing.html>.
- [23] D. P. Kingma and J. Ba, "Adam: A Method for Stochastic Optimization," *arXiv preprint arXiv:1412.6980*, 2014.
- [24] S. Mallat, *A wavelet tour of signal processing*. Elsevier, 1999.
- [25] R. Caromi, M. Souryal, and T. A. Hall, "Rf dataset of incumbent radar signals in the 3.5 ghz cbrs band," *Journal of Research of the National Institute of Standards and Technology*, vol. 124, p. 1, 2019.
- [26] MATLAB, "LTE Toolbox," https://www.mathworks.com/help/lte/index.htmls_tid=CRUX_lftnav.
- [27] F. Chollet *et al.*, "Keras," <https://keras.io>, 2015.